RSC Advances

PAPER

View Article Online
View Journal | View Issue

Cite this: *RSC Adv.*, 2020, **10**, 29031

Lignin nanoparticles are renewable and functional platforms for the concanavalin a oriented immobilization of glucose oxidase–peroxidase in cascade bio-sensing†

Eliana Capecchi,[a] Davide Piccinino,[a] Elisabetta Tomaino,[a] Bruno Mattia Bizzarri,[a] Francesca Polli,[b] Riccarda Antiochia,[b] Franco Mazzei[b] and Raffaele Saladino *[a]

Received 20th May 2020
Accepted 23rd July 2020

DOI: 10.1039/d0ra04485g

rsc.li/rsc-advances

Lignin nanoparticles (LNPs) acted as a renewable and efficient platform for the immobilization of horseradish peroxidase (HRP) and glucose oxidase (GOX) by a layer by layer procedure. The use of concanavalin A as a molecular spacer ensured the correct orientation and distance between the two enzymes as confirmed by Förster resonance energy transfer measurement. Layers with different chemo–physical properties tuned in a different way the activity and kinetic parameters of the enzymatic cascade, with cationic lignin performing as the best polyelectrolyte in the retention of the optimal Con A aggregation state. Electrochemical properties, temperature and pH stability, and reusability of the novel systems have been studied, as well as their capacity to perform as colorimetric biosensors in the detection of glucose using ABTS and dopamine as chromogenic substrates. A boosting effect of LNPs was observed during cyclovoltammetry analysis. The limit of detection (LOD) was found to be better than, or comparable to, that previously reported for other HRP–GOX immobilized systems, the best results being again obtained in the presence of a cationic lignin polyelectrolyte. Thus renewable lignin platforms worked as smart and functional devices for the preparation of green biosensors in the detection of glucose.

Introduction

Lignin nanoparticles (LNPs), the most abundant and renewable polyphenol in nature,[1–4] have received great attention due to the emergence of novel rheological and chemo–physical properties with respect to the amorphous counterpart.[5–8] These properties are associated with π–π supramolecular organization of the polymer chain during the nanostructuration process, yielding head-to-tail (J-type)[9,10] and tail-to tail (H-type)[11] aggregates of the aromatic moieties. The π–π interactions favor the occurrence of electron and charge transfer processes[12,13] providing novel redox and chemical patterns. For this reason, LNPs have been applied as renewable and functional platform for the immobilization of redox enzymes, such as laccase,[14] tyrosinase,[15] and horseradish peroxidase,[16] and of hydrolase.[17] LNPs exerted a specific boosting effect in the case of laccase by both long-range electron transfer (pseudo-DET) and mediated electron transfer (MET) mechanisms.[18] Similarly, lignin boosted the activity of monooxygenase in the degradation of recalcitrant polyphenols thanks to the formation of low molecular weight frameworks[19] as diffusible redox mediators.[20,21] The immobilization of enzymatic cascade is a relevant tool to achieve complex molecular architectures mimicking the natural spatial organization of the enzymes in the cell.[22–25] Intrinsic advantages of these supramolecular arrangements are an improved catalytic efficacy,[26] the fast transportation of key intermediates between the active sites,[27] and the limitation of the occurrence of mass transfer diffusion barriers.[28] In this way, activity, selectivity, stability, and reusability of the enzymatic cascade is optimized.[29]

The reciprocal orientation of the active site in the cascade is an important feature to control the overall activity of the system.[30] For this reason, specific molecular spacers and linkers are used[31,32] for orienting the enzymes in the proper way.[33]

Here we report that LNPs are green and suitable platform for the immobilization of the enzymatic cascade of Horseradish Peroxidase (HRP) and Glucose Oxidase (GOX)[34,35] in biosensing applications.[36,37] To the best of our knowledge, only examples of the use of hybrid systems encompassing unstructured lignin and metal oxides have been previously reported for the immobilization of GOX.[38,39] The correct orientation of the two enzymes during the immobilization process was obtained by the use of the lectin Concanavalin A (Con A), able to selectively

[a]*Department of Biological and Ecological Sciences (DEB), University of Tuscia, via S. Camillo de Lellis, 01100 Viterbo, Italy. E-mail: saladino@unitus.it*

[b]*Department of Chemistry and Drug Technologies, Sapienza University of Rome, P.le Aldo Moro 5, Rome, 00185, Italy*

† Electronic supplementary information (ESI) available. See DOI: 10.1039/d0ra04485g

interact with the carbohydrate part of both HRP and GOX.[40] Since the carbohydrate component of glycoproteins is usually far from the active site of the enzyme, the use of Con A ensures the retention of the enzymatic activity, sometimes enhancing the performance of the system.[41,42] The effectiveness of Con A in the immobilization of HRP alone on LNPs has been recently reported, focusing on bio-desulfurization processes.[16] The overall immobilization procedure of the enzymatic cascade was based on two different approaches: (i) direct adsorption on the surface of LNPs; (ii) layer by layer (LbL) mediated adsorption in the presence of cationic polyelectrolytes including poly(diallyl dimethylammonium chloride) (PDDA), chitosan (CH) and cationic lignin (CATLIG). These polyelectrolytes have been selected on the basis of their previous application in the coating of LNPs,[8,14] two of them (PDDA and CH) being also reported in the formation of aggregates with Con A.[43,44] CATLIG is the cationic form of lignin with relevant application in the stabilization of pickering emulsions[45] and in the immobilization of different enzymes.[16–18] Förster resonance energy transfer (FRET) measurement[46] confirmed the co-immobilization of HRP and GOX on LNPs, the two enzymes being located at the optimal distance. The application of natural and renewable polyelectrolytes CH and CATLIG is in accordance with the development of a full green system. LNPs showed a boosting effect in the electrocatalytic activity of the enzymatic cascade as evaluated by cyclic voltammetry analysis. The biosensing application of immobilized HRP/GOX enzymatic cascade has been measured by the colorimetric detection of β-D-glucose using two chromogenic substrates, 2,2′-azinobis-(3-ethylbenzothiazoline-6-sulfonic acid) (ABTS) and dopamine. The limit of detection (LOD) was found to be better than, or comparable to, that previously reported for other HRP/GOX immobilized systems.

Results and discussion

Procedure for the immobilization of HRP and GOX on LNPs

LNPs have been prepared starting from commercially available organosolv lignin by applying the nanoprecipitation procedure.[47] Briefly, a solution of the raw lignin in tetrahydrofuran (THF) was rapidly added to deionized water with instantaneous formation of the nanoparticles[18] (scanning electron microscopy image of LNPs is reported in ESI SI #1, Fig. S1†). The immobilization procedure of HRP and GOX is reported in Scheme 1. In the first case (pathway A), Con A from jack beans (*Canavalia ensiformis*) was adsorbed on the surface of LNPs by treating the nanoparticles (1.5 mg mL^{-1}) in sodium phosphate buffer (PBS, 1.0 mL; pH 7.3, 0.1 M) with different concentration of Con A (from 0.2 mg mL^{-1} to 1.0 mg mL^{-1}) in the same buffer (1.0 mL) at 25 °C. The tetrameric configuration of Con A necessary for the molecular recognition of glycoproteins was preserved by buffering the pH of the system (pH 7.3).[48]

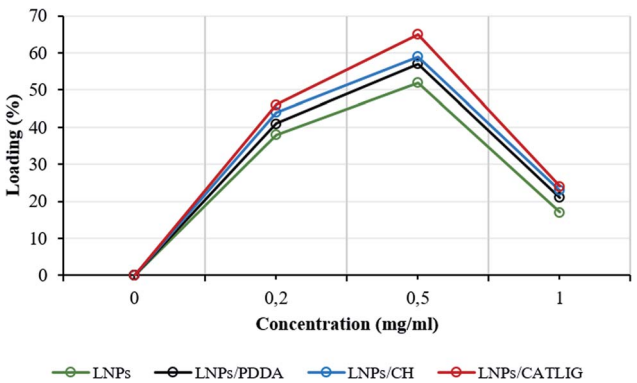

Fig. 1 Loading of Con A on LNPs during different adsorption procedures. The loading factor is defined as % in weight of Con A per mg of LNPs. LNPs, LNPs/PDDA, LNPs/CH or LNPs/CATLIG intermediates are represented with a color code (green line, black line, blue line and red line, respectively). All experiments were conducted in triplicate. The average error in protein concentration parameters is *c.a.* 1.2%.

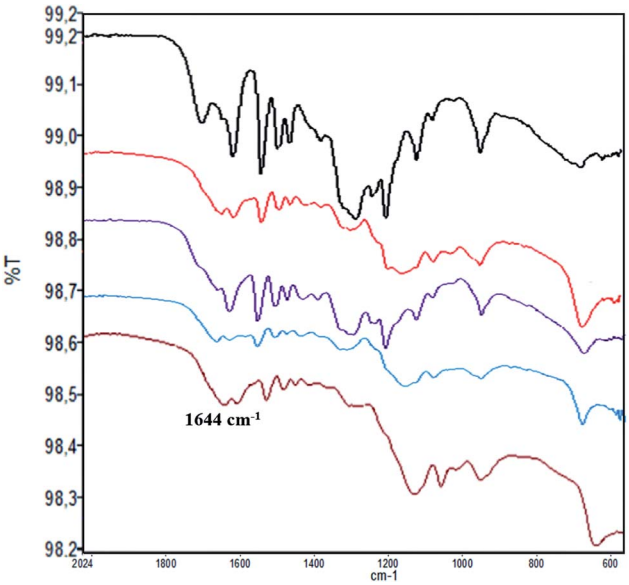

Fig. 2 ATR FT-IR analysis of LNPs/Con A and LNPs/polyelectrolyte/Con A samples. LNPs alone: black line; LNPs/Con A: red line; LNPs/PDDA/Con A: purple line; LNPs/CH/Con A: azure line; LNPs/CATLIG/Con A: brown line. The presence of Con A was associated to the appearance of the amide I band in the spectrum (*c.a.* 1.644 cm^{-1}).

The efficacy of the adsorption of Con A was evaluated by the Bradford assay on the residual solution after removal of the nanoparticles.[49] The interaction between lectins and polyphenols is reported, mainly focusing on their relevance for nutraceutical aspects.[50]

The loading factor (% in weight) of Con A on LNPs is reported in Fig. 1. The highest efficacy in the immobilization process was obtained starting from 0.5 mg mL^{-1} of Con A (Fig. 1, green line). Attenuated total reflection Fourier transform infrared (ATR FT-IR) analysis confirmed the effectiveness of the immobilization of Con A on LNPs, as shown by the appearance of the amide I band in the spectrum (1.644 cm^{-1}) associated to the characteristic stretching amide vibrational mode (amide II band) (Fig. 2). The LNPs/Con A intermediate (1.5 mg mL^{-1}) in PBS (1.0 mL) was treated with HRP (2.5 mg mL^{-1}) and GOX (5.0 mg mL^{-1}) in PBS (20 μL) at 4.0 °C, applying the optimal HRP/GOX ratio value previously reported for the co-

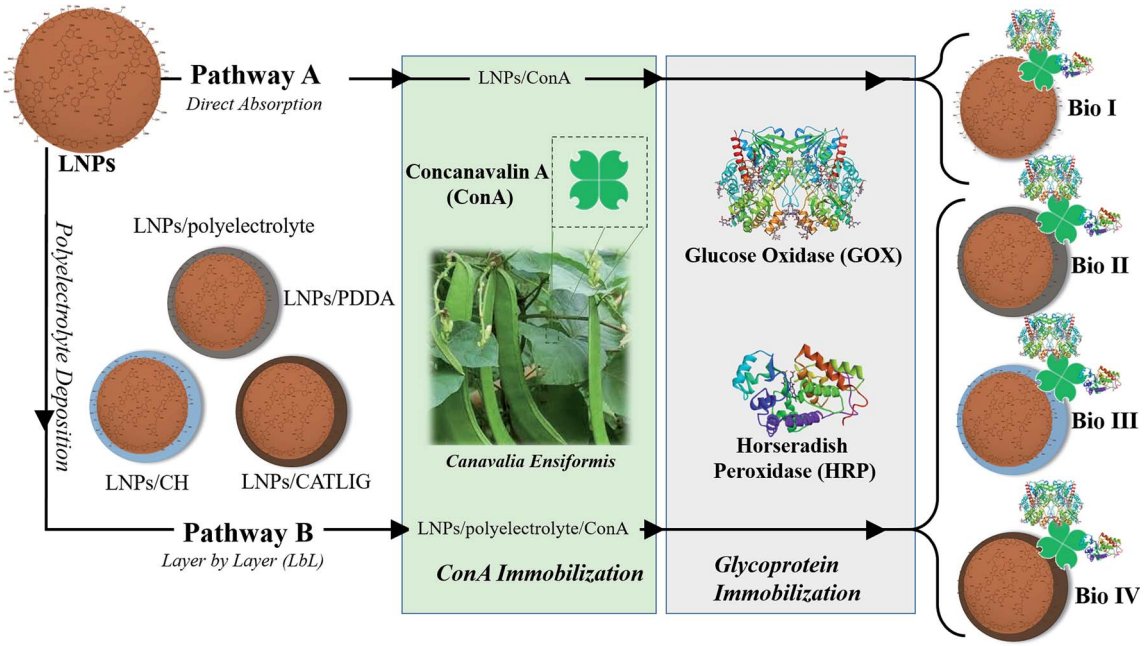

Scheme 1 Schematic representation of the immobilization of HRP and GOX on LNPs. Pathway A: direct adsorption on the surface of LNPs; pathway B: layer by layer (LbL) mediated adsorption in the presence of different cationic polyelectrolytes. Grey color: PDDA; azure color: CH; dark brown color: CATLIG.

immobilization of the two enzymes on Con A in homogeneous conditions[51] to yield LNPs/Con A/HRP–GOX system **Bio I**.

As an alternative, LNPs were coated with cationic polyelectrolyte to favor the electrostatic interaction with negative charged Con A (ζ-potential, −14 mV (ref. 52)) (Scheme 1, pathway B). LNPs (1.0 mg mL^{-1}) in deionized water (1.0 mL) were treated with the appropriate polyelectrolyte poly (diallyl dimethylammonium chloride) (PDDA), chitosan (CH), and cationic lignin (CATLIG) (1.0 mg mL^{-1}, 0.5 mg mL^{-1}, and 0.1 mg mL^{-1}, respectively), in deionized water (1.0 mL) at 25 °C under orbital shaking. The optimal concentration of the polyelectrolyte was selected on the basis of previous reported data.[8,18]

The intermediates, LNPs/PDDA, LNPs/CH and LNPs/CATLIG (1.5 mg mL^{-1}) in PBS (1.0 mL) were added with different concentration of Con A (from 0.2 mg mL^{-1} to 1.0 mg mL^{-1}) in the same buffer (1.0 mL) at 25 °C. The highest loading values were obtained in the presence of 0.5 mg mL^{-1} of Con A irrespective to the nature of the polyelectrolyte (Fig. 1), CATLIG being the best support for all of the tested concentrations. Dynamic light scattering (DLS) data for original LNPs, LNPs/CATLIG and LNPs/CATLIG/Con A, as selected examples, are reported in the ESI (SI #2) and in Fig. S2.† LNPs showed an average size of diameter of 219 nm.[53] After the deposition of CATLIG the diameter value was slightly increased to 234 nm, reaching the value of 244 nm in the presence of Con A. This trend was in accordance with previous reported data.[42,45] The optimal value of concentration of Con A was then selected for the further study. The presence of the polyelectrolyte generally increased the efficacy of the Con A loading.

ATR FT-IR analysis of LNPs/polyelectrolyte/Con A intermediates confirmed the presence of Con A (Fig. 2) (ATR FT IR spectra of LNPs/polyelectrolyte intermediates are reported in SI #3, Fig. S3†).

The successive treatment of LNPs/polyelectrolyte/Con A intermediates (1.5 mg mL^{-1}) in PBS (1.0 mL) with HRP (2.5 mg mL^{-1}) and GOX (5.0 mg mL^{-1}) in PBS (20 μL) at 4.0 °C afforded LNPs/PDDA/Con A/HRP–GOX **Bio II**, LNPs/CH/Con A/HRP–GOX **Bio III**, and LNPs/CATLIG/Con A/HRP–GOX **Bio IV**, respectively (Scheme 1). The scanning electron microscopy images of **Bio I–IV** are reported in Fig. 3 (panel A–F). **Bio I–IV** showed a regular spherical shape after the deposition procedure. The magnification of **Bio I** and **Bio IV** highlight the typical corona-like structural motif associated to Con A.[41]

Activity parameters and kinetic data of Bio I–IV

The activity parameters and kinetic data of **Bio I–IV** are reported in Table 1. The data were recorded following the activity of HRP as a quantitative marker of the overall enzymatic cascade process, firstly activated by the GOX oxidation of β-D-glucose to β-D-glucone lactone with concomitant production of hydrogen peroxide (H_2O_2).[54] The efficacy of HRP in the reduction of H_2O_2 was then measured by the 2,2′-azinobis-(3-ethylbenzothiazoline-6-sulfonic acid) (ABTS) assay,[51,55] following the concentration of the corresponding ABTS radical cation (415 nm) at 25 °C, and working at the optimal pH value for the activity of both HRP and GOX (pH 7.0).[56] The selection of HRP as representative component of the HRP–GOX cascade system is widely reported, the two enzymes having similar reaction rates.[57,58] The activity yield and immobilization yield were determined using eqn (1) and (2), respectively:

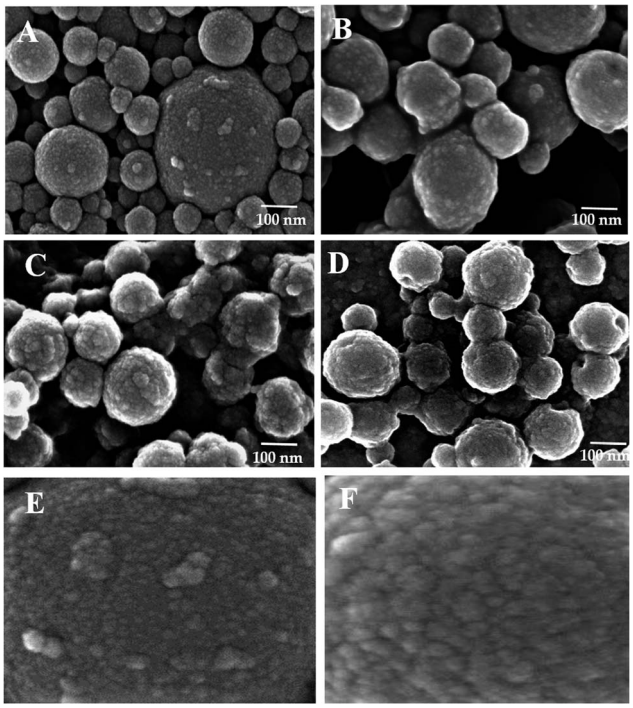

Fig. 3 Scanning electron microscopy images of **Bio I** (panel A), **Bio II** (panel B), **Bio III** (panel C), and **Bio IV** (panel D). Panel E and F: magnification (×800 K) of **Bio I** and **Bio IV**, respectively.

$$\text{Activity yield (\%)} = [U_x/(U_a - U_r)] \times 100 \quad (1)$$

$$\text{Immobilization yield (\%)} = [(U_a - U_r)/U_a] \times 100 \quad (2)$$

where U_a is the total activity (units) of co-immobilized HRP, U_r is the residual HRP activity (units) in the solution and U_x is the activity of HRP after the co-immobilization process (the enzyme unit is the increase in the absorbance of 10^{-3} unit per min at 25 °C in 0.1 M PBS). Notably, the random immobilization of HRP and GOX on LNPs without the use of Con A, both in the presence or in the absence of the polyelectrolyte, afforded systems deprived of any catalytic activity (the detailed procedure for the preparation of these reference systems, including Table S1† reporting the loading value of the two enzymes in the different samples, are reported in SI #4†). This result is in accordance with previously reported data on the relevance of the spatial distribution for the catalytic activity of the enzymes during the immobilization processes.[59–62] The cationic polyelectrolyte layers favored the Con A mediated immobilization yield of HRP and GOX (Table 1, entries 3–5 *versus* entry 2), CATLIG being the most effective polyelectrolyte (Table 1, entry 5 *versus* entries 3 and 4). As a general trend, the polyelectrolyte layer increased the activity yield, with the only exception of PDDA. The overall effect was more pronounced in the case of CATLIG (Table 1, entry 5). The kinetic data (K_m, V_{max}, and K_{cat}) of **Bio I–IV** have been compared with the performance of the two enzymes loaded on Con A under similar experimental conditions but in the absence of LNPs (Con A/HRP–GOX).[51] As reported in Table 1, **Bio IV** showed always the highest V_{max} and K_{cat} values (Table 1, entry 5 *versus* entries). Moreover, **Bio I** and **Bio III** were characterized by V_{max}values similar to Con A/HRP–GOX, having a lower K_{cat}. Finally, **Bio II** was the lowest active system. Note that, in the case of layered samples, better results were obtained with polyelectrolytes characterized by a ζ-potential value comprised between +20 mV and +10 mV (CATLIG and CH, respectively).[63,64] Apparently, the higher value of the ζ-potential reported for PDDA (+40 mV)[65] was detrimental for the overall activity of the system. Probably, the catalytic efficiency of **Bio I–IV** was dependent on the modality of the loading of Con A, due to the occurrence of supramolecular interactions tuning the optimal tetrameric configuration of the lectin. In accordance with this hypothesis, the effect of cationic polyelectrolytes in the stability and aggregation behavior of Con A has been reported in relation to the formation of amyloid fibrils,[66,67] able to control the transition of Con A from the optimal β-sheet configuration to less effective α-helices.[68]

Table 2 Activity retained after different temperature condition and reusability test of **Bio I**, **III** and **IV**

		Activity yield (%)						
				Reusability[a] (%)				
Entry	Sample	25 °C	60 °C	Run 1	Run 2	Run 3	Run 4	Run 5
1	**Bio I**	52	44	42	31	28	25	23
2	**Bio III**	55	53	44	39	34	31	30
3	**Bio IV**	61 (60)[b]	60	59	57	55	54	52

[a] The experiment was performed by recovery of **Bio I**, **III** and **IV** analyzing their reuse for five runs with freshly prepared glucose and ABTS solutions in PBS (pH 7.0, 0.1 M). [b] Activity of **Bio IV** after 30 days of storage in PBS solution at 5 °C.

Table 1 Activity and kinetic parameters of **Bio I–IV**[a]

Entry	Sample	Immobilization yield (%)	Activity yield (%)	K_m[c] (mM)	V_{max}[c] (μmol L^{-1} s^{-1})	K_{cat}[c] (s^{-1})
1	Con A/HRP–GOX[b]	—	—	17.26	0.12	594
2	**Bio I**	88	52	8.72	0.10	563
3	**Bio II**	91	51	4.77	0.07	284
4	**Bio III**	93	55	8.30	0.13	576
5	**Bio IV**	96	61	4.85	0.15	652

[a] **Bio I**: LNPs/Con A/HRP–GOX; **Bio II**: LNPs/PDDA/Con A/HRP–GOX; **Bio III**: LNPs/CH/HRP–GOX; **Bio IV**: LNPs/CATLIG/HRP–GOX. [b] Con A/HRP–GOX was used as reference.[49] [c] Kinetic data (K_m, V_{max} and K_{cat}) were analyzed by GraphPad software. Average errors in kinetic parameters were 2–4% for K_m, 1–3% for V_{max} and 1–2% for K_{cat}. The experiments were carried out in triplicate.

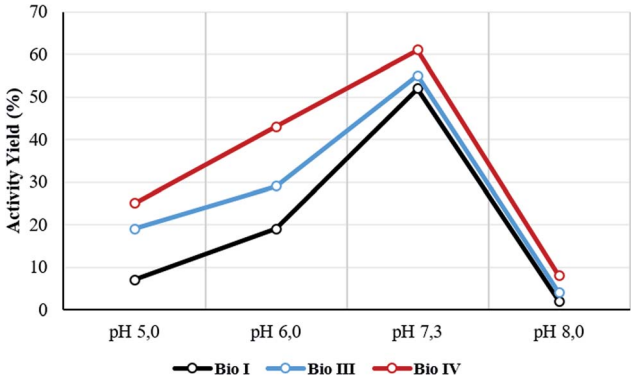

Fig. 4 pH stability of Bio I, III and IV. The pH range was controlled by sodium acetate buffer (pH 5.0–6.0) and PBS (pH 7.3–8.0). The pH stability of Bio I, III and IV are represented with a color code (black line, azure line and red line, respectively). All experiments were conducted in triplicate. The average error in activity yield calculation is *c.a.* 1.5%.

The alteration of the β-sheet configuration might be also responsible for the lower activity of **Bio I** with respect to Con A/HRP–GOX, since it is reported that low molecular weight polyphenols interact with Con A by H-bonding and hydrophobic forces at the rigid β-sheet responsible for the stabilization of the canonical tetrameric structure.[69]

Temperature and pH stability, and reusability assay

The temperature and pH stability, and reusability assay, were evaluated for the most active **Bio I**, **III** and **IV**. The activity yield for the selected samples was measured at 60 °C and at different pH values (from pH 5 to pH 8). Data are reported in Table 2 and Fig. 4, respectively. The systems showed a high thermal stability (from 85% to 99% of retained activity, respectively), **Bio IV** being the most stable device (Table 2, entries 1–3). As reported in Fig. 4, irrespective from the experimental conditions, the optimal value of the activity yield was observed in the range of pH value between 6.0 and 7.5, the highest performance being always obtained at pH 7.3. Again, **Bio IV** performed as the best system. The time stability of the most active system **Bio IV** was evaluated by measuring the activity of the system after 30 days of storage in PBS solution at 5 °C. Under these experimental conditions, **Bio IV** retained the original activity (Table 2, entry 3).

The reusability of **Bio I**, **III** and **IV** was then evaluated by recovering the sample at the end of the oxidation, followed by washing and successive new runs. The systems maintained a significative activity yield after five runs (Table 2, reusability expressed in % with respect to the initial value), the better result being obtained with **Bio IV** (52% of the initial activity).

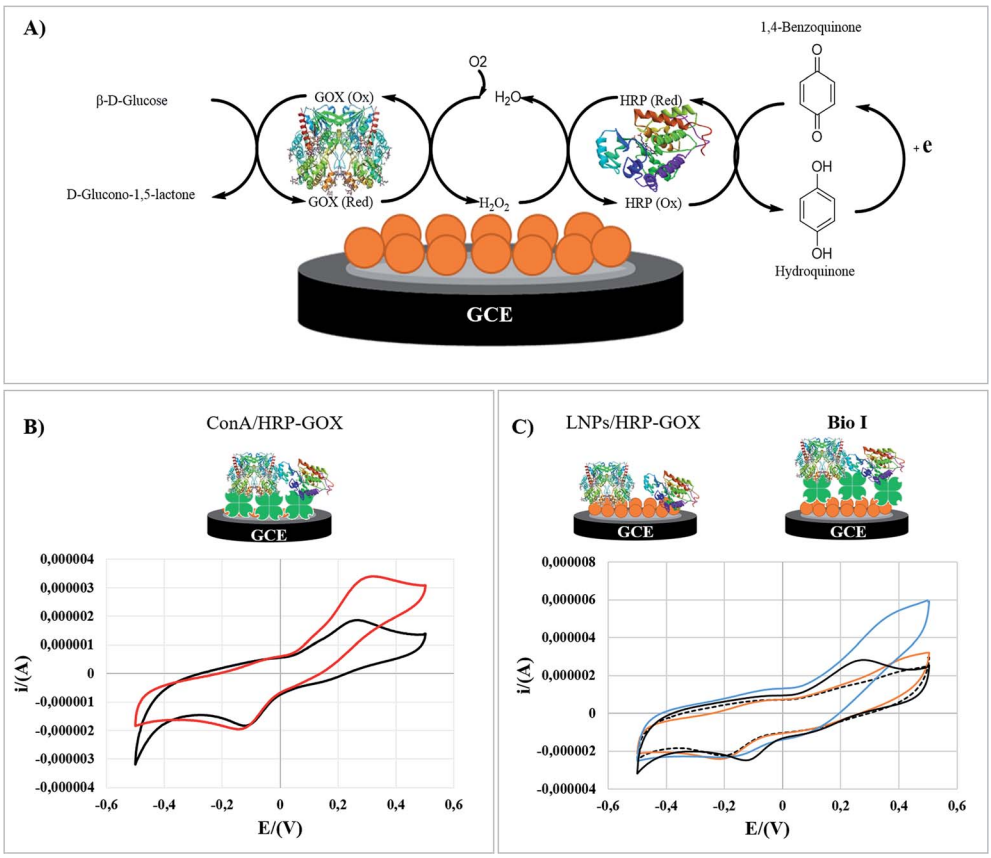

Fig. 5 Cyclic voltammetry analysis of Con A/HRP–GOX compared to Bio I and the random immobilization of HRP and GOX on LNPs without the use of Con A. Panel A: reaction scheme of cascade reaction. Panel B: Con A/HRP–GOX and hydroquinone in absence and in presence of glucose (black line and red line, respectively). Panel C: LNPs/HRP–GOX and hydroquinone in absence and in presence of glucose (black dashed line and orange line, respectively) and Bio I and hydroquinone in absence and in presence of glucose (black line and blue line, respectively).

Electrochemical characterization

Bio I was analyzed by cyclic voltammetry (CV) as a representative example to elucidate the role of Con A in the electrocatalytic activity of the enzymatic cascade after the immobilization on LNPs. The electrochemical behavior of original LNPs (SI #5†) was in accordance with data previously reported.[70,71] The experiments were performed in hydroquinone solution (H_2Q) as electroactive mediator (1.0×10^{-4} M, PBS, 50 mM; pH 7.0), in the absence and presence of glucose (1.0×10^{-2} M) (the detailed procedure is reported in the experimental part). Cyclic voltammograms (CVs) have been recorded with a glassy carbon electrode (GC) reproducing **Bio I**, as shown in Fig. 5 (panel C). The overall bioelectrode performance was regulated by the oxidation of H_2Q to 1,4-benzoquinone on the electrode surface, following the cascade reaction of HRP and GOX. The schematic representation of the enzymatic transformations occurring at the surface of the GC electrode is reported in Fig. 5 (panel A).

Con A/HRP–GOX (panel B) and LNPs/HRP–GOX (panel C) have been used as references. The electrochemical response of each system was compared with that obtained in the absence of glucose, corresponding to the cyclic voltammograms of H_2Q alone (black curves, panels B and C). The voltammetry curves of LNPs/HRP–GOX and **Bio I** in the absence of glucose showed a similar behavior, **Bio I** showing a slightly higher electrochemical responsiveness. The cyclic voltammogram of Con A/HRP–GOX with H_2Q solution showed an irreversible behavior as highlighted by the separation between the cathodic and anodic peaks (*c.a.* 360 mV; panel B, black curve). However, in the presence of LNPs/HRP–GOX and **Bio I** the electrochemical behavior appeared to be more reversible, with a peak-to-peak potential separation of about 150 mV, indicating the occurrence of a quasi-reversible two-electron transfer reaction (panel C, black curve). The anodic and cathodic peak currents were linearly related to $\nu^{1/2}$, thus meaning a typical diffusion-controlled process (data not shown). The diffusion coefficient (D) was calculated to be 5.2×10^{-4} cm^2 s^{-1}, higher than that reported in the literature for a bare glassy carbon electrode.[72] Hence, LNPs increased the electrochemical performance independently from the presence of Con A.

This result can be ascribed to the electrochemical responsiveness of LNPs, which allows a better electron transfer mechanism at the electrode surface.[73] Successively, the electrocatalytic activity of the three systems was studied by adding glucose. The Con A/HRP–GOX showed a clear electrocatalytic responsiveness in the presence of glucose, confirming the retained activity of HRP and GOX after immobilization of Con A (Fig. 5, panel B. red curve).

The beneficial role of Con A was further highlighted by the comparison of the CVs of **Bio I** and LNPs/HRP–GOX (Fig. 5, panel C). In this latter case, the presence of Con A assured the highest electrocatalytic effect (blue curve), a slight

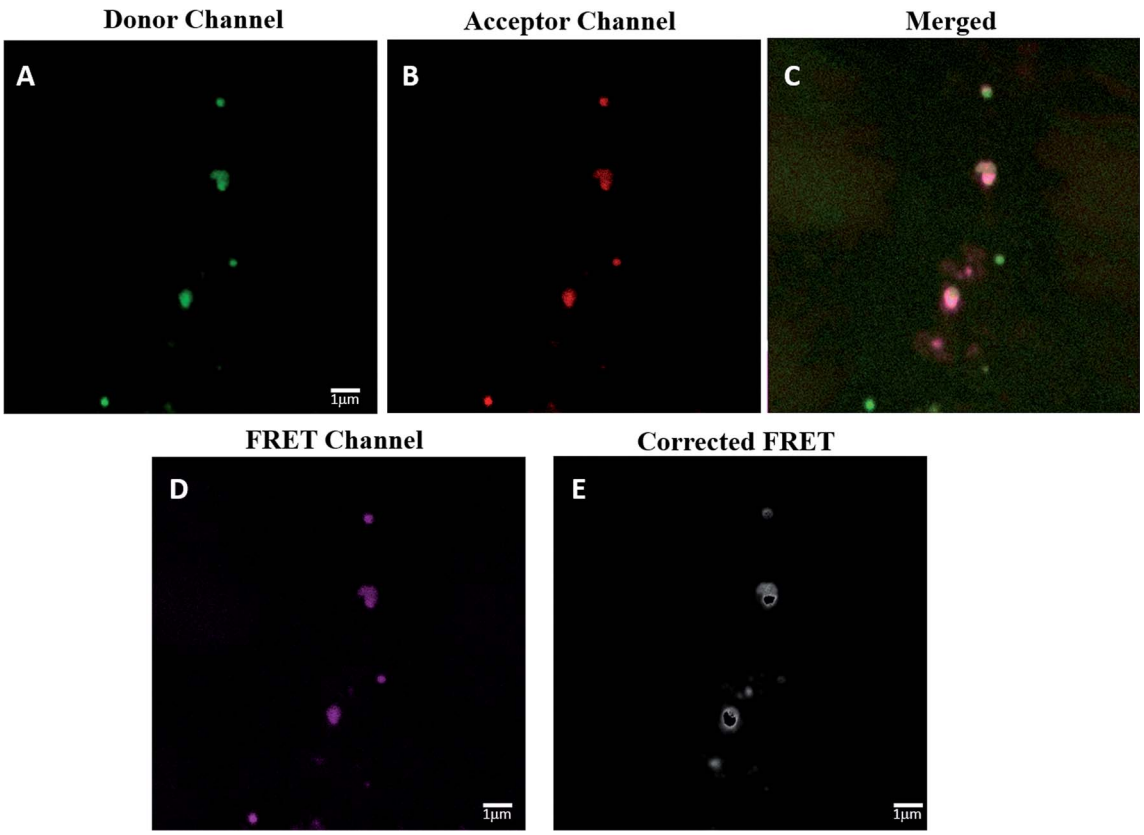

Fig. 6 Laser confocal scanning microscopy of Bio IV. Panel A: HRP labelled with FITC in the donor channel at 490 nm (green pixels). Panel B: GOX labelled with RhoB in the acceptor channel at 560 nm (red pixels). Panel C: merged fluorescence effect. Panel D: original FRET signal. PANEL E: corrected FRET signal.

electrochemical responsiveness being observed for the LNPs/HRP–GOX counterpart (orange curve). Note that LNPs played a boosting effect in the activity of the overall system, the CV of **Bio I** showed an electrocatalytic effect higher than simple Con A/HRP–GOX (Fig. 5, panel C *versus* panel B). Boosting effect exerted by lignin on the activity of oxidases are reported in literature.[19] Probably, this effect may be due to the improved stability of the system, even if the amplification of the electrochemical signal by electron transfer processes occurring in the aromatic structure of LNPs cannot be completely ruled out.[12,13]

Förster resonance energy transfer (FRET) analysis

The spatial distance between HRP and GOX in the most active **Bio IV** was determined by confocal laser scanning microscopy (CLSM) analysis associated to Förster resonance energy transfer (FRET) effect (Fig. 6, panel A–D). FRET signal in CLSM occurs between two proximately located fluorophores *via* non-radiative dipole–dipole coupling as a consequence of the energy transfer between a donor and an acceptor dye in close proximity (3–10 nm).[74] The application of the FRET analysis in the study of bio-molecular conformation, protein–protein interaction and molecular motor devices has been reported.[75,76] In the case of **Bio IV**, HRP was labeled with fluorescein isothiocyanate (FITC) as donor, while GOX was labeled with rhodamine B (RhoB) and worked as the acceptor counterpart.[77] The labelling procedure of HRP and GOX is reported in SI #6.†

The effective presence of FITC-HRP in **Bio IV** was detected in the donor channel mode at 490 nm (Fig. 6 panel A, green fluorescence signal), while that of RhoB–GOX was detected in the acceptor channel mode at 560 nm (Fig. 6 panel B, red fluorescence signal). The effective co-localization of HRP–GOX in **Bio IV** was highlighted by the presence of the merged fluorescent signal (Fig. 6, panel C). The original and corrected FRET signals of **Bio IV** (Fig. 6, panel D and E, respectively) were used to calculate the average distance between the donor and the acceptor moieties (details for the FRET calculation are reported in SI #6†). HRP and GOX were located at the distance of 7.0 nm, a value that is comprised in the range of reported optimal distances for the activity of the enzymatic cascade.[62]

Evaluation of Bio I, III and IV as colorimetric biosensor

The performance of **Bio I**, **III** and **IV** as colorimetric biosensors was first evaluated by using the ABTS assay.[51] Briefly, the appropriate sample (1.0 mg) in PBS (0.1 M, pH 7, 3.0 mL) was treated with ABTS (0.5 mM, 0.1 mL) in the presence of different

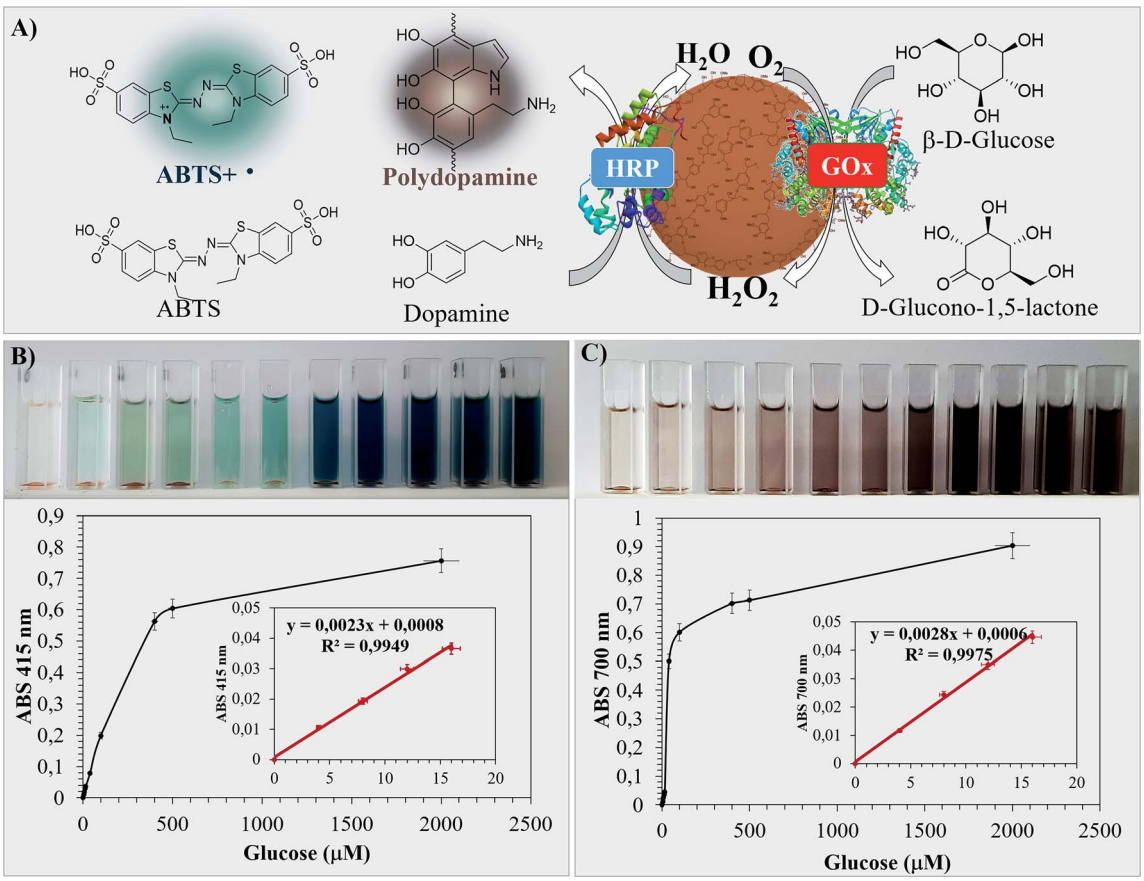

Fig. 7 ABTS and dopamine colorimetric assay of **Bio IV**. Panel A: schematic representation of the cascade oxidation of β-D-glucose by **Bio IV** in the presence of ABTS or dopamine. The structure of the chromogenic products is reported with a different color code. Panel B: color change variation and absorbance trend (415 nm) during the ABTS assay. Panel C: color change variation and absorbance trend (700 nm) during the dopamine assay. Linear trends and correlation coefficient values are magnified in both panels. The error bars indicate the standard deviation of three replicate of the measurement.

Table 3 Limit of detection value (LOD) for Bio I, III and IV

		LOD[a] (μM)	
Entry	Sample	ABTS	Dopamine
1	HRP–GOX[b]	5.43	2.39
2	Con A/HRP–GOX	5.10	3.25
3	**Bio I**	3.90	1.20
4	**Bio III**	1.71	1.14
5	**Bio IV**	1.21	0.85

[a] The LOD was evaluated as reported in literature.[78] [b] Homogeneous HRP–GOX mixture (same ratio value than that used for the Bio systems).

concentrations of β-D-glucose (from 4.0 μM to 2000 μM). The absorbance of the ABTS radical cation produced during the HRP–GOX oxidation was monitored at 415 nm after 30 min at 25 °C. The data of the most active **Bio IV** are reported in Fig. 7, corresponding data for **Bio I** and **Bio III** are in SI #7.† The homogeneous HRP–GOX mixture (same ratio value than that used for the bio systems) and Con A/HRP–GOX were used as references. The color of the solution changed significantly during the addition of β-D-glucose from pale azure to deep blue and dark indigo (Fig. 7, panel B). The variation of the absorbance with respect to β-D-glucose concentration was used for the determination of the limit of detection (LOD), taking into account the linear part of the curve.[78] The linear trend of **Bio IV** was found to be comprised between 4.0 μM and 16 μM, corresponding to a linear correlation coefficient $R^2 = 0.9949$ and a LOD value of 1.21 μM (Table 3, entry 5). **Bio IV** showed a LOD value lower than **Bio I**, **Bio III** and references (Table 3, entry 5 *versus* entries 1–4). This result confirmed the relevance of the ordered deposition of the two enzymes on the lignin platform. Note that the shape of **Bio IV** particles was unchanged after the biosensing application, as evaluated by SEM analysis (SI #8, Fig. S6†).

As an alternative, the LOD was evaluated by following the oxidation of L-dopamine as a natural chromogenic compound. The oxidation of L-dopamine by HRP and H_2O_2 to yield black polydopamine in quantitative yield has been reported.[79] In this latter case the LOD was found to be significantly lower than that obtained with other standard chromogenic compounds.[80] The oxidation of L-dopamine with **Bio IV** was performed under the experimental conditions previously reported for ABTS. The colorimetric variation during the addition of β-D-glucose and the respective absorbance values at 700 nm are in Fig. 7 (panel C) (LOD values of **Bio I** and **Bio III** are in Table 3, the corresponding absorbance curves are in SI #7†). As reported in Table 3, **Bio IV** showed lower LOD value with respect to the ABTS assay. Again, the LOD of **Bio IV** was lower than that of **Bio I** and **Bio III**, and of the two reference systems (Table 3, entry 5 *versus* entries 1–4).

Experimental

Materials

Organosolv lignin (OL), were purchased from Chemical Point (Oberhaching, Germany). Glucose oxidase (GOX, from *Aspergillus niger*, 160 kDa, catalytic activity according to producer specification is 100–250 U per mg), horseradish peroxidase (HRP, from *Armoracia Rusticana*, 44 kDa, catalytic activity according to producer specification is 173 U per mg), concanavalin A (Con A, from *Canavalia ensiformis*, Jack bean type VI), poly(diallyldimethylammonium chloride) PDDA (20% v/v water solution), chitosan (CH, low molecular weight, 75–85% deacetylated degree, 50–190 kDa), were purchased from Sigma-Aldrich. Cationic lignin (CATLIG) was prepared from organosolv lignin (10 mg mL; 0.1 M) in NaOH, by treatment with glycidyl tetramethyl ammonium chloride (20 mg) at 60 °C for 2 h under magnetic stirring. The crude was purified for 24 hours by dialysis with Spectrapore™ membrane (3.5 kDa molecular weight cut off). Bradford reagent, 2,2-azinobis-(3-ethylbenzothiazoline-6-sulfonic acid) (ABTS) and β-D-glucose were purchased from Sigma-Aldrich. L-dopamine were purchased from TCI Europe. All experiments were performed in phosphate buffer saline (PBS, 0.1 M, pH 7.3 or pH 8.0), or sodium acetate buffer (0.1 M, pH 5.0 or pH 6.0), prepared by using Milli-Q water ($\rho = 18.2$ MΩ cm a 25 °C; TOC < 10 μg L^{-1}, Millipore, Molsheim, France).

Procedure for the preparation of Bio I

Lignin nanoparticles (LNPs) were prepared from organosolv lignin (OL) by using the nanoprecipitation procedure.[47] Briefly, a solution of OL (2.0 mg in 1.2 mL of tetrahydrofuran (THF)/H_2O 2 : 1 v/v) was added to Milli-Q water (3.8 mL) to yield LNPs. The LNPs dispersion was concentrated using a rotary evaporator in order to remove the organic solvent, frozen and lyophilized. LNPs (1.5 mg) in PBS (1.0 mL) were treated with Con A (0.5 mg) in PBS (1.0 mL, 0.1 M; pH 7.3) in order to obtain the LNPs/Con A intermediate. LNPs/Con A was added to a solution of HRP (0.12 mg mL^{-1}) and GOX (0.25 mg mL^{-1}) in PBS (1.0 mL, 0.1 M; pH 7.3) and left under orbital shaking at 4 °C for 24 h. LNPs/Con A/HRP–GOX **Bio I** was isolated by centrifugation (20 min at 6000 rpm), washed with sodium phosphate buffer (1.0 mL, 0.1 M; pH 7.3) and lyophilized, while the residual solution was evaluated for the immobilization yield and activity parameters.

Procedure for the preparation of Bio II–IV

LNPs/polyelectrolyte intermediates were prepared by treatment of LNPs (1.0 mL Milli-Q water; 1.0 mg mL^{-1}) with the appropriate amount of poly(diallyldimethylammonium chloride) (PDDA), chitosan (CH), or cationic lignin (CATLIG) (1.0 mg mL^{-1}, 0.5 mg mL^{-1}, and 0.1 mg mL^{-1}, respectively), in deionized water (1.0 mL) at 25 °C under orbital shaking for 2 hours. The corresponding LNPs/PDDA, LNPs/CH and LNPs/CATLIG were isolated by centrifugation and lyophilized. Concanavalin A was adsorbed on the surface of the appropriate LNPs/polyelectrolyte (1.5 mg) in PBS (1.0 mL) by treating with Con A (0.5 mg) in PBS (1.0 mL, 0.1 M; pH 7.3) in order to obtain LNPs/polyelectrolyte/Con A intermediates.

LNPs/polyelectrolyte/Con A was added to a solution of HRP (0.12 mg mL^{-1}) and GOX (0.25 mg mL^{-1}) in PBS (1.0 mL, 0.1 M; pH 7.3) and left under orbital shaking at 4 °C for 24 h. **Bio II–IV** were isolated by centrifugation (20 min at 6000 rpm), washed

with sodium phosphate buffer (1.0 mL, 0.1 M; pH 7.3) and lyophilized, while the residual solution was evaluated for the immobilization yield and activity parameters.

Bradford assay

The loading of Con A on LNPs (defined as % in weight of Con A per mg of LNPs) obtained during the different procedures was evaluated by the Bradford assay of the appropriate residual solution. The Con A concentration was calculated spectrophotometrically at 595 nm by using the Bradford reagent and bovine serum albumin as reference protein.

Activity and kinetic parameters

The ABTS spectrophotometric assay was used for the determination of the enzymatic activity of Con A/HRP–GOX and **Bio I–IV** by following the absorbance at 415 nm ($\varepsilon_{415} = 36\,000\ M^{-1}\ cm^{-1}$) for 10 minutes. In a typical experiment, Con A/HRP–GOX and **Bio I–IV** (0.1 mg in PBS, 0.1 M, pH 7.0, 3.0 mL), were added to ABTS (0.5 mM) and β-D-glucose (100 mM). The activity unit of HRP in the enzymatic cascade was considered as the amount of enzyme able to transforms 1.0 μmole of H_2O_2 per min at pH 7 at 25 °C. Kinetic parameters (K_m, V_{max}, and K_{cat}) were determined by measuring the activity at different concentrations of β-D-glucose (0−100 mM) using the ABTS assay. As a general procedure, the reaction was started by adding β-D-glucose to PBS solution containing the appropriate amount of the sample (0.1 mg in PBS, 0.1 M, pH 7.0, 3.0 mL). The data were analysed by Lineweaver–Burk plots, the initial velocities ($1/V$ *vs.* $1/[S]$) and K_m and V_{max} being calculated as intercepts at the cartesian axes, respectively. The Michaelis–Menten constant and the turnover number have been calculated performing the analysis in triplicate by the use of the GraphPad software.

Temperature and pH stability and reusability assay

Temperature and pH stability, and reusability assay were performed by using a slightly modified procedure of the ABTS spectrophotometric test. In particular, the temperature stability was determined by adding **Bio I**, **III** and **IV** (0.1 mg in PBS, 0.1 M, pH 7.0, 3.0 mL) to a solution of ABTS (0.5 mM) and β-D-glucose (100 mM) in an oil bath at 60 °C and monitoring the absorbance at 415 nm for 10 minutes. For the pH stability, the appropriate amount of **Bio I**, **III** and **IV** (0.1 mg) was added to buffer solution (3.0 mL) at different pH values (sodium acetate buffer 0.1 M, at pH 5.0 and at pH 6.0, PBS 0.1 M at pH 7.3 and at pH 8.0), containing the appropriate solution of ABTS (0.5 mM) and β-D-glucose (100 mM). The production of the cation radical of ABTS was monitored at 415 nm for 10 minutes at 25 °C. The reusability of **Bio I**, **III** and **IV** was performed under the experimental condition described above. At the end of the transformation, **Bio I**, **III** and **IV** were recovered by centrifugation and washed three times with deionized water in order to eliminate the residual ABTS. After all, **Bio I**, **III** and **IV** were reused with fresh glucose/ABTS solution for five consecutive runs.

Electrochemical characterization of Bio I, Con A/HRP–GOX, LNPs/HRP–GOX

The immobilization procedure for the development of modified glassy carbon electrodes (GCE) with **Bio I**, Con A/HRP–GOX and LNPs/HRP–GOX was performed by a sequential layer-by-layer drop-casting procedure. In particular, for **Bio I**, a three step drop casting procedure was performed as follow: LNPs (15 μL, 1.5 mg mL^{-1}) in PBS (50 mM, pH 7.0) was sonicated for 5 minutes, the dispersion was drop-cast onto the (GCE) and let it dry for 20 minutes. Successively, a solution of Con A (15 μL, 0.5 mg mL^{-1}) was drop-cast onto the electrode surface and let it dry for 20 minutes. The electrode was then rinsed with PBS 50 mM pH 7.0. Finally, HRP (15 μL, 0.12 mg mL^{-1}) and GOX (15 μL, 0.25 mg mL^{-1}) in PBS (50 mM, pH 7.0), was drop-cast onto the electrode surface and let it dry for 30 minutes. The electrode surface was then rinsed with PBS. The GCE/Con A/HRP–GOX system was prepared under the experimental conditions previously reported for **Bio I** without the LNPs drop-casting. The GCE/LNPs/HRP–GOX system was prepared under the experimental conditions previously reported for **Bio I** without the Con A drop-casting. The voltammetric experiments were performed at room temperature in PBS (50 mM, pH 7.0), using hydroquinone solution (H_2Q), as the electroactive mediator (1.0×10^{-4} M, PBS, 50 mM; pH 7.0), in the absence and presence of β-D-glucose (1.0×10^{-2} M) and in a potential range between −0.5 and 0.5 V at a scan rate of 100 mV s^{-1}. All electrochemical measurements were carried on with a PGSAT204N potentiostat (Eco Chemie, Utrecht) controlled by the Nova 2.1 software with a conventional three electrodes configuration. A saturated calomel electrode (SCE, 244 mV *vs.* NHE, Cat. 303/SCG/12, AMEL, Milan, Italy) as reference, a glassy carbon rod electrode (d = 2 mm, Cat. 6.1241.020, Metrohm, Herisau, Switzerland) as counter and a glassy carbon (GC) as working electrode (d = 3 mm, Cat. 6.1204.300, Metrohm, Herisau, Switzerland). Before functionalization, GCE was polished for 10 minutes using alumina slurries with two different particle size (0.3 μm/0.05 μm) using cloth pads wet with Milli-Q water, rinsed with Milli-Q water, and further sonicated for 5 min between each polishing step.

Colorimetric performance of Bio I, III and IV

The colorimetric analysis was performed by using different concentrations of β-D-glucose (from 4.0 μM to 2000 μM) into cuvettes containing the appropriate amount of **Bio I**, **III** and **IV** (1.0 mg, in PBS 0.1 M, pH 7.0, 3.0 mL) and ABTS (0.5 mM, 0.1 mL) or L-dopamine (0.5 mM, 0.1 mL) as chromogenic substrates. After 30 minutes under magnetic stirring at 25 °C the dispersion was photographed with a digital camera and the corresponding absorption spectra were measured by a UV-Vis spectrophotometer (Varian Cary® 50 UV-Vis) setting the wavelength at 415 nm and 700 nm for ABTS and L-dopamine, respectively.

ATR FT-IR analysis

LNPs/Con A and LNPs/polyelectrolyte/Con A samples were analyzed by attenuated total reflection Fourier transform

Table 4 Limit of detection value (LOD) for **Bio I** compared to other biosensing systems

Entry	Device	Chromogenic substrates	LOD (μM)
1	HRP–GOX copper based nanoparticles[37]	TMB[a]	25
2	HRP–GOX inorganic nanocrystal[78]	ABTS	0.3
3	HRP–GOX zinc adenine complex[81]	ABTS	1.84
4	**Bio IV** (this work)	L-dopamine	0.85

[a] 3,3′,5,5′-Tetrametilbenzidine.

infrared (ATR-IR) spectroscopic using a PerkinElmer (Spectrum One) spectrometer (UATR unit cell) averaging 32 scans (resolution of 4 cm^{-1}).

Scanning electron microscopy

The field emission scanning electron microscopy (FESEM) of **Bio I–IV** was acquired on FESEM ZEISS GeminiSEM500, operated at 5 kV after drop 20 μL (with deionized water) of sample dispersion on specimen stubs, air dried and coated with gold by sputtering with AGAR (Auto Sputter Coater). Before the observations, the sample received a deposition of chromium thin film (5 nm) by sputter coating using a QUORUM Q 150T ES plus coater.

Confocal laser microscopy, FRET

The detailed procedure for the labeling of HRP and GOX and for the calculation of the FRET effect are reported in SI #6.† The confocal images of **Bio IV** were obtained by ZEISS LSM-710 NLO confocal system equipped with a Plan Apochromat 100×/1.40 oil DIC M 27 objectives was used for laser confocal microscopy.

Conclusions

LNPs proved to be an efficient green platform for the immobilization of HRP and GOX mediated by Con A. The activity and kinetic parameters of the HRP–GOX enzymatic cascade were controlled by the specific nature of the cationic polyelectrolyte layer able to modify the aggregation stability of the tetrameric sub-units of Con A, CATLIG being the best performing polyelectrolyte. In this latter case, the optimal distance of 7.0 nm was measured between immobilized HRP and GOX by Förster resonance energy transfer (FRET) effect. Cyclic voltammetry analysis confirmed the critical role played by Con A in the electrochemical responsiveness of the systems, associated to a boosting effect exerted by LNPs probably due a better electron transfer mechanism occurring at the electrode surface. The efficacy of novel immobilized Con A/HRP–GOX systems in the oxidation of β-D-glucose was tested by colorimetric assay, using ABTS and dopamine as chromogenic substrates. The lowest LOD values were obtained in the presence of CATLIG as cationic polyelectrolyte layer. Table 4 reports the comparison of the LOD value for **Bio IV** with that of other reference systems. In particular, a LOD value (0.85 μM) better than, or comparable to, that previously reported for other heterogeneous HRP–GOX immobilized systems was observed.[37,78,81] The fact that a full renewable nanoplatform composed by lignin (organosolv and CATLIG) and Con A can efficiently support the HRP–GOX enzymatic cascade maintaining the catalytic activity open a new entry for a green and biodegradable family of biosensors useful for bio-catalytic and environmentally friendly applications.

Conflicts of interest

There are no conflicts to declare.

Acknowledgements

The authors acknowledge the EU project-EASME/EMFF/Blue Economy-2018/n.863697 “FISH chitinolytic biowastes FOR FISH active and sustainable packaging material” (FISH4-FISH)”.Dr Lorenzo Arrizza and Microscopies center of L'Aquila University are acknowledged for SEM analyses. The Large Equipment Center (CGA) of Tuscia University are acknowledged for confocal analysis and FRET measurements.

References

1 P. S. Chauhan, *Bioresour. Technol.*, 2020, **9**, 100374.
2 W. G. Glasser, *Front. Chem.*, 2020, **7**, 565.
3 W. Zhao, B. Simmons, S. Singh, A. Ragauskas and G. Cheng, *Green Chem.*, 2016, **18**, 5693–5700.
4 I. Siavash and S. V. Rajender, *Green Chem.*, 2020, **22**, 612–636.
5 Z. Ma, C. Liu, N. Niu, Z. Chen, S. Li, S. Liu and J. Li, *ACS Sustainable Chem. Eng.*, 2018, **6**, 3169–3175.
6 W. Yang, E. Fortunatia, F. Bertoglio, J. S. Owczarek, G. Brunif, M. Kozanecki, J. M. Kenny, L. Torre, L. Visai and D. Puglia, *Carbohydr. Polym.*, 2018, **181**, 275–284.
7 W. Yang, E. Fortunati, F. Dominici, G. Giovanale, A. Mazzaglia, G. M. Balestra, J. M. Kenny and D. Puglia, *Eur. Polym. J.*, 2016, **79**, 1–12.
8 D. Piccinino, E. Capecchi, L. Botta, B. M. Bizzarri, P. Bollella, R. Antiochia and R. Saladino, *Biomacromolecules*, 2018, **19**, 3883–3893.
9 Y. Deng, X. Feng, M. Zhou, Y. Qian, H. Yu and X. Qiu, *Biomacromolecules*, 2011, **12**, 1116–1125.
10 Y. Deng, X. Feng, D. Yang, C. Yi and X. Qiu, *BioResources*, 2012, **7**, 1145–1156.
11 F. C. Spano and C. Silva, *Annu. Rev. Phys. Chem.*, 2014, **65**, 477–500.
12 G. A. Di Labio and E. R. Johnson, *J. Am. Chem. Soc.*, 2007, **129**, 6199–6203.

13 A. Batra, G. Kladnik, H. Vázquez, J. S. Meisner, L. Floreano, C. Nuckolls, D. Cvetko, A. Morgante and L. Venkataraman, *Nat. Commun.*, 2012, **3**, 1086.
14 E. Capecchi, D. Piccinino, B. M. Bizzarri, D. Avitabile, C. Pelosi, C. Colantonio, G. Calabrò and R. Saladino, *Biomacromolecules*, 2019, **20**, 1975–1988.
15 E. Capecchi, D. Piccinino, I. Delfino, P. Bollella, R. Antiochia and R. Saladino, *Nanomaterials*, 2018, **6**, 438.
16 E. Capecchi, D. Piccinino, B. M. Bizzarri, L. Botta, M. Crucianelli and R. Saladino, *Catalysts*, 2020, **10**, 313.
17 M. H. Sipponen, M. Farooq, J. Koivisto, A. Pellis, J. Seitsonen and M. Österberg, *Nat. Commun.*, 2018, **9**, 2300.
18 D. Piccinino, E. Capecchi, L. Botta, P. Bollella, R. Antiochia, M. Crucianelli and R. Saladino, *Catal. Sci. Technol.*, 2019, **9**, 4125–4413.
19 M. Frommhagen, S. K. Mutte, A. H. Westphal, M. J. Koetsier, S. W. A. Hinz, J. Visser, J. P. Vincken, D. Weijers, W. J. H. Van Berkel, H. Gruppen and M. A. Kabel, *Biotechnol. Biofuels*, 2017, **10**, 121.
20 L. Brenelli, F. B. Squina, C. Felby and D. Cannella, *Biotechnol. Biofuels*, 2018, **11**, 1.
21 E. Kim, W. T. Leverage, Y. Liu, I. M. White, W. E. Bentley and G. F. Payne, *Analyst*, 2014, **139**, 32–43.
22 A. Giannakopoulou, E. Gkantzou, A. Polydera and H. Stamatis, *Trends Biotechnol.*, 2020, **38**, 202–216.
23 C. Schmid-Dannert and F. López-Gallego, *Curr. Opin. Chem. Biol.*, 2019, **49**, 97–104.
24 J. Muschiol, C. Peters, N. Oberleitner, M. D. Mihovilovic, U. T. Bornscheuer and and F. Rudroff, *Chem. Commun.*, 2015, **51**, 5798–5811.
25 K. Ariga, Q. Ji, T. Mori, M. Naito, Y. Yamauchi, H. Abe and J. P. Hill, *Chem. Soc. Rev.*, 2013, **42**, 6322–6345.
26 M. Filice and J. M. Palomo, *ACS Catal.*, 2014, **4**, 1588–1598.
27 Y. H. P. Zhang, *Biotechnol. Adv.*, 2011, **29**, 715–725.
28 T. S. Schwarzer, L. Klermund, G. Wang and K. Castiglione, *Nanotechnology*, 2018, **29**, 44.
29 F. Lopez-Gallego, *Methods Enzymol.*, 2019, **617**, 385–411.
30 S. Schoffelen and J. C. Van Hest, *Curr. Opin. Struct. Biol.*, 2013, **23**, 613–621.
31 Y. Liu, T. L. Ogorzalek, P. Yang, M. M. Schroeder, E. N. G. Marsh and Z. Chen, *J. Am. Chem. Soc.*, 2013, **135**, 12660–12669.
32 J. Turková, *J. Chromatogr. B: Biomed. Sci. Appl.*, 1999, **722**, 11–31.
33 J. Huang, W. Zhuang, C. Wei, L. Mu, J. Zhu, Y. Zhu and H. Ying, *Process Biochem.*, 2018, **64**, 160–169.
34 F. Jia, S. K. Mallapragada and B. Narasimhan, *Ind. Eng. Chem. Res.*, 2015, **54**, 10212–10220.
35 O. Idan and H. Hess, *Curr. Opin. Biotechnol.*, 2013, **24**, 606–611.
36 H. H. Nguyen, S. H. Lee, U. J. Lee, C. D. Fermin and M. Kim, *Materials*, 2019, **12**, 121.
37 X. Zhu, J. Huang, J. Liu, H. Zhang, J. Jiang and R. Yu, *Nanoscale*, 2017, **9**, 5658–5663.
38 M. Stanisz, Ł. Klapiszewski and T. Jesionowski, *Chem. Eng. J.*, 2020, **397**, 125409.
39 A. Jędrzak, T. Rębiś, M. Kuznowicz and T. Jesionowski, *Int. J. Biol. Macromol.*, 2019, **127**, 677–682.
40 H. Yao, Q. Gan, J. Peng, S. Huang, M. Zhu and K. Shi, *Sensors*, 2016, **16**, 563.
41 Y. Yong, R. Su, X. Liu, W. Xu, Y. Zhang, R. Wang and Z. Liu, *Biochem. Eng. J.*, 2018, **129**, 26–32.
42 W. Xu, Y. Yong, Z. Wang, G. Jiang, J. Wu and Z. Liu, *ACS Sustainable Chem. Eng.*, 2016, **5**, 90–96.
43 L. Chen, Y. Fu, N. Wang, A. Yang, Y. Li, J. Wu and F. Yan, *ACS Appl. Mater. Interfaces*, 2018, **10**, 18470–18477.
44 A. F. Che, Z. M. Liu, X. J. Huang, Z.-G. Wang and Z. K. Xu, *Biomacromolecules*, 2008, **9**, 3397–3403.
45 M. H. Sipponen, M. Smyth, T. Leskinen, L.-S. Johansson and M. Österberg, *Green Chem.*, 2017, **19**, 5831–5840.
46 F. Wu and S. D. Minteer, *Biomacromolecules*, 2013, **14**, 2739–2749.
47 T. Leskinen, M. Smyth, Y. Xiao, K. Lintinen, M. L. Mattinen, M. A. Kostiainen and M. Österberg, Nord Pulp Pap, *J. Res.*, 2017, **32**, 586–596.
48 X. Xu, Y. Yuan, G. Hu, X. Wang, P. Qi, Z. Wang and H. Yang, *Sci. Rep.*, 2017, **7**, 1452.
49 T. Spector, *Anal. Biochem.*, 1978, **86**, 142–146.
50 B. C. Fish and L. U. Thompson, *J. Agric. Food Chem.*, 1991, **39**, 727–731.
51 Y. Zhang, Y. Yong, J. Ge and Z. Liu, *ACS Catal.*, 2016, **6**, 3789–3795.
52 A. Makky, J. P. Michel, P. Maillard and V. Rosilio, *Biochim. Biophys. Acta Rev. Biomembr.*, 2011, **1808**, 656–666.
53 S. Beisl, J. Adamcyk and A. Friedl, *Molecules*, 2020, **25**, 1388.
54 L. T. Nguyen and K. L. Yang, *Enzyme Microb. Technol.*, 2017, **100**, 52–59.
55 R. Saladino, M. Guazzaroni, C. Crestini and M. Crucianelli, *ChemCatChem*, 2013, **5**, 1407–1415.
56 G. Palazzo, G. Colafemmina, C. Guzzoni Iudice and and A. Mallardi, *Sens. Actuators, B*, 2014, **202**, 217–223.
57 J. L. Lin, L. Palomec and I. Wheeldon, *ACS Catal.*, 2014, **4**, 505–511.
58 D. Simon, F. Obst, S. Haefner, T. Heroldt, M. Peiter, F. Simon and D. Appelhans, *React. Chem. Eng.*, 2019, **4**, 67–77.
59 O. Idan and H. Hess, *Curr. Opin. Biotechnol.*, 2013, **24**, 606–611.
60 V. Hitaishi, R. Clement, N. Bourassin, M. Baaden, A. de Poulpiquet, S. Sacquin-Mora and E. Lojou, *Catalysts*, 2018, **8**, 192.
61 J. Fu, Y. R. Yang, A. Johnson-Buck, M. Liu, Y. Liu, N. G. Walter and H. Yan, *Nat. Nanotechnol.*, 2014, **9**, 531–536.
62 A. Kuzmak, S. Carmali, E. von Lieres, A. J. Russell and S. Kondrat, *Sci. Rep.*, 2019, **9**, 1.
63 G. N. Rivière, A. Korpi, M. H. Sipponen, T. Zou, M. A. Kostiainen and M. Österberg, *ACS Sustainable Chem. Eng.*, 2020, **8**, 4167–4177.
64 F. P. Ramanery, A. A. Mansur and H. S. Mansur, *Nanoscale Res. Lett.*, 2013, **8**, 512.
65 M. Mayer, D. Dedovets, Y. Guari, J. Larionova, J. Long and J. Causse, *J. Colloid Interface Sci.*, 2017, **505**, 364–372.

66 J. M. Khan, M. S. Khan, A. Qadeer, M. A. Alsenaidy, A. Ahmed, N. A. Al-Shabib and R. H. Khan, *Colloids Surf.*, 2017, **522**, 494–502.
67 S. K. Chaturvedi, J. M. Khan, M. K. Siddiqi, P. Alam and R. H. Khan, *Int. J. Biol. Macromol.*, 2016, **83**, 315–325.
68 J. M. Khan, M. R. Khan, P. Sen, A. Malik, M. Irfan and R. H. Khan, *J. Mol. Liq.*, 2018, **269**, 796–804.
69 B. A. M. Rocha, C. S. Teixeira, J. C. Silva-Filho, R. B. Nóbrega, D. B. Alencar, K. S. Nascimento and P. Delatorre, *Int. J. Biol. Macromol.*, 2015, **72**, 1136–1142.
70 D. H. Nagaraju, T. Rebis, R. Gabrielsson, A. Elfwing, G. Milczarek and O. Inganäs, *Adv. Energy Mater.*, 2013, **4**, 1300443.
71 K. Gawluk, A. Modrzejwska-Sikorska, T. Rębiś and G. Milczarek, *Catalysts*, 2017, **7**, 392.
72 T. Kamgaing, K. I. Tonle and Y. F. Emanbou, *J. Anal. Chem.*, 2013, **8**, 64–77.
73 V. K. Thakur, M. K. Thakur, P. Raghvan and P. Kessler, *ACS Sustainable Chem. Eng.*, 2014, **2**, 1072–1092.
74 P. C. Ray, Z. Fan, R. A. Crouch, S. S. Sinha and A. Pramanik, *Chem. Soc. Rev.*, 2014, **43**, 6370–6404.
75 Y. He, Y. Li, S. Mukherjee, Y. Wu, H. Yan and H. P. Lu, *J. Am. Chem. Soc.*, 2011, **133**, 14389–14395.
76 W. M. Shih, Z. Gryczynski, J. R. Lakowicz and J. A. Spudich, *Cell*, 2000, **102**, 683–694.
77 Y. Zhang, F. Lyu, J. Ge and Z. Liu, *Chem. Commun.*, 2014, **50**, 12919–12922.
78 Z. Li, Y. Zhang, Y. Su, P. Ouyang, J. Ge and Z. Liu, *Chem. Commun.*, 2014, **50**, 12465–12468.
79 A. Palumbo, A. Napolitano, P. Barone and M. d' Ischia, *Chem. Res. Toxicol.*, 1999, **12**, 1213–1222.
80 J. Li, M. A. Baird, M. A. Davis, W. Tai, L. S. Zweifel, K. M. A. Waldorf and X. Gao, *Nat. Biomed. Eng.*, 2017, **1**, 6.
81 H. Liang, S. Sun, Y. Zhou and Y. Liu, *Catalysts*, 2017, **7**, 327.